CSCE Annual Conference

Growing with youth – Croître avec les jeunes

Laval (Greater Montreal)

June 12 - 15, 2019

FRP MATERIALS FOR REHABILITATION OF BURIED PIPES

Kanagaraj, Anita Shiny [1] and Sadeghian, Pedram [1,2]

[1] Department of Civil and Resource Engineering, Dalhousie University, Canada

[2] Pedram.Sadeghian@dal.ca

Abstract: Over time, pipes tend to deteriorate due to various physical and chemical parameters. Therefore, they necessitate rehabilitation to improve the service life of structure. Bonding a fiber-reinforced polymer (FRP) liner inside the pipe, is an effective rehabilitation technique to increase the strength and stiffness of deteriorated pipes. To do so, it is very important to know the structural behavior and mechanical properties of the FRP liner under applied loads. This paper discusses the results of solid wall FRP liners with four layers of fabric, subjected to compressive transverse loading. A customized compression testing machine with string potentiometers to measure the diametrical change was set up to test the liners under parallel-plate loading test method. Four specimens of glass fiber-reinforced polymer (GFRP) and two specimens of carbon fiber-reinforced polymer (CFRP) liners, having an average internal diameter of 330 mm and 336 mm respectively, were tested to find the diametrical change, stiffness factor (SF) and pipe stiffness (PS) at 5% and 10% diametrical change. Based on experimental results it was evident that, due to changing stiffness and large deformations under loading, the specimens experienced geometric non-linearity. An analytical model was developed to find diametrical deflections both in vertical and horizontal directions and their corresponding strains at springline and crown/invert to elucidate the elliptical ring deflection causing the geometric non-linearity. The model seemed to be in good agreement with the test results.

1 INTRODUCTION

Pipes are primarily used as culverts, storm water drains, sewers, water conduits, storage tanks and tunnels. Exposure to various physical and chemical parameters causes the pipes to deteriorate as they age. This leads to a decrease in strength, durability and service life of the pipes. Based on previous studies by Ehsani and Pena (2009) and Simpson et al. (2017), an effective method to rehabilitate such pipes is by bonding fiber-reinforced polymer (FRP) liners inside the pipes. Lining the pipes would also improve properties such as corrosion resistance, temperature resistance and resistance against chemical attacks. FRP'S are highly preferred for this purpose because of their high strength-to-weight ratio/ specific strength, dimensional stability, low installation and maintenance cost, durability over a range of conditions and good mechanical properties. A notable aspect of these materials is the smoothness they provide which directly translates to less friction, thereby resisting scale deposits and allowing an efficient pipe flow. Unlike the conventional grout technique used for rehabilitation, FRP liners do not reduce the cross-sectional flow area of the pipe significantly and an effective discharge can be ensured.

Studies on FRP liners based on sectional ring tests, external load test for Three-Edge Bearing (TEB) strength and full-scale hydrostatic burst test, for the purpose of pipe rehabilitation have been conducted by Lee and Karbhari (2005) previously. This study was an effort to bridge the gap in understanding the behaviour of FRP liners under compressive transverse loading and analyse the ring deflection without finite element modelling but basic mechanics. The fabricated FRP liners were tested under this loading to study their mechanical properties and structural behavior and to predict the pipe stiffness and stiffness factor

according to ASTM D2412 -11 standards. On subjecting the liners to loading, they undergo a consecutive elliptical diametrical deflection. Elliptical deformation reduces the moment of inertia of the cross-section and the liner will experience a high induced stress when compared to the original circular cross-section, which relates to lowered mechanical integrity (Park et al. 2014; Lee et al. 2015; Rafiee and Habibagahi 2018). This will have a negative impact on the transmission and conveyance of materials in the pipe. According to Rafiee and Habibagahi (2018), estimating and analyzing the stiffness of liners during the design stages and prior to the establishment of mass production, is one of the fundamental issues from both structural and functional point of views. In this study, four GFRP and two CFRP liner specimens were fabricated and tested under parallel plate loading test. The diametrical deflection, PS, SF and strength were determined. An analytical model was developed to validate the elliptical deformation and strains at springline and crown/invert that contributes to the geometric non-linearity.

2 EXPERIMENTAL STUDY

2.1 Test Matrix

Four GFRP and two CFRP specimens with an average internal diameter of 330 mm and 360 mm and width of 315 mm, respectively were fabricated. Four layers of fabric with an overlap of 100 mm approx. were cured in epoxy resin for both liner types. More details are provided as test matrix in Table 1. The test specimens were identified with a specimen ID as GS/CS – X, where G stands for glass fiber, C stands for carbon fiber, S stands for solid wall and X denotes the ID number. For example, GS – 01 stands for GFRP solid wall specimen with ID number 1.

Table 1: Test matrix

Specimen ID	Internal Diameter (mm)	Width (mm)
GS-01	329.75	309.00
GS-02	343.25	320.13
GS-03	338.50	313.00
GS-04	344.63	318.38
CS-01	347.63	316.38
CS-02	346.75	315.63

2.2 Material Properties

The liners consisted of four layers of unidirectional glass/carbon fabric saturated using a two-component epoxy resin. The aerial weight of glass fabric was 915 g/m^2. It had a tensile strength of 3.24 GPa, tensile elastic modulus of 72.4 GPa, density of 2.55 g/cm^3 and rupture strain of 4.5%. When the glass fabric was laminated with epoxy, the ply thickness was 1.3 mm and had an tensile strength of 587 MPa and the elastic modulus was 27.4 GPa. The carbon fabric had a dry fabric weight of 943 g/m^2, tensile strength of 3.8 GPa, tensile modulus of 231 GPa, density of 1.8 g/cm^3, ultimate elongation of 1.64%. When laminated with epoxy, the carbon fabric had a ply thickness was 1.24 mm and a tensile strength of 782 MPa and elastic modulus of 100 GPa. The viscosity of two-component saturating resin was 1500-1600 cps. It was mixed in 2:1 ratio with 2 parts of resin and 1 part of hardener. The full cure time was 48 hours and had a tensile strength, compressive strength and flexural strength of 49.3 MPa, 65.4 MPa and 76.8 MPa respectively. The tensile modulus, compressive modulus and flexure modulus were 1.995 GPa, 3.25 GPa and 1.740 GPa respectively. Also, the water absorption was <1% in 24 hours. All the material properties of dry fiber, laminate and epoxy are as specified by the manufacturer QuakeWrap Inc., Tucson, AZ, USA.

2.3 Specimen Fabrication

While producing the liner specimens, sheets of glass and carbon fabric were cut to required length using shears. Cutting out large dimension sheets, helped in fabricating four pipe liners at once. Wet lay-up method was used to fabricate all the specimens. The fabric was thoroughly cleaned to avoid any dust particles. A plastic sheet was laid over a cardboard liner mould of 12 in. (305 mm) nominal diameter, before placing the

fabric. The fabric was then placed in four layers with an end overlap of 4 in. (100 mm). A roller was used to evenly distribute the resin over the fabric surface and a spatula was used to smoothen the resin layer. A motor system was used to rotate slowly the wet specimen to create a small centrifugal force, such that the resin doesn't concentrate at the bottom. The specimens cured for approximately 24 hours at room temperature with a plastic sheet covering its exposed surface, to obtain a smooth and dust free surface, then the cardboard mould and plastic sheets were removed. After at least 7 days of curing at room temperature, the single unit of liner was cut into four identical specimens using a diamond-bladed saw. The rough edges were slightly sanded to obtain a smooth surface. A measuring tape was used to measure the internal diameter and the width, and a digital caliper was used to measure the thickness of each specimen at eight different locations and was averaged for further calculations.

2.4 Test Setup and Instrumentation

For testing the liners, a customized parallel-plate load test setup was made using a 20 kN load cell. The plates were 450 x 750 mm in size and had a thickness of ½ in. (12.7 mm). The stroke of actuator was 340 mm and pump allowed a loading rate of 20 mm/min. Two strain gauges (SG) were applied at mid-height of the liner on the crown and invert positions. Two strain gauges were applied on either exterior side of the liner at springline position as shown below. All strain gauges were placed parallel to the fiber direction.

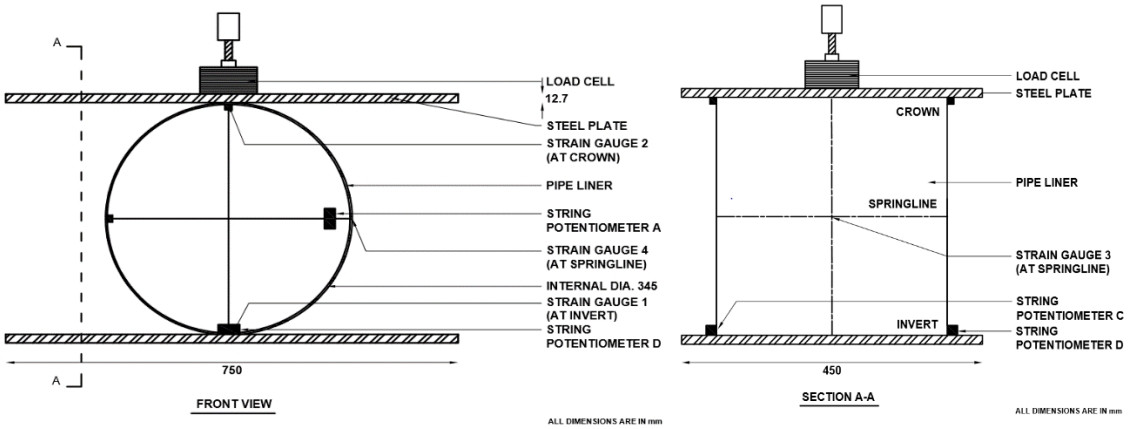

Figure 1: Test setup and instrumentation

The fabricated specimen was attached with a string potentiometer on sides A and B which could measure up to 635 mm deflection in the horizontal direction, by drilling small holes on either side of the liners. Likewise, string potentiometers C and D were clamped to top and bottom plate respectively and could measure a deflection of up to 305 mm in the vertical direction. All the specimens were then tested under compressive transverse loading. Displacements (Vertical and Horizontal) and Strains (Springline and Crown/Invert tensile strain) were collected using a data acquisition system.

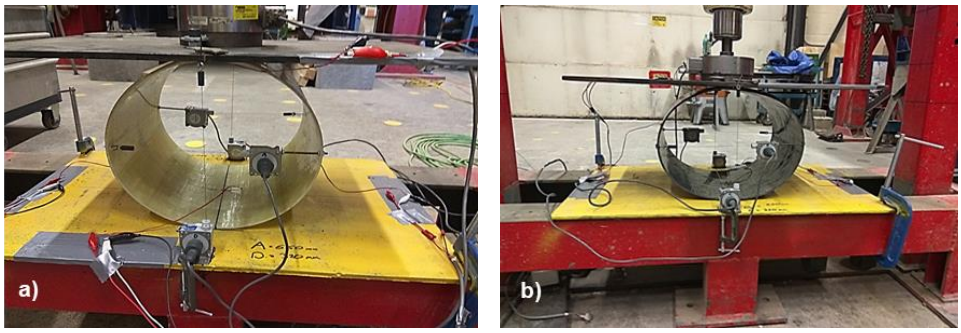

Figure 2: Test Setup (a) GFRP Liner; and (b) CFRP Liner

3 RESULTS AND DISCUSSION

3.1 Failure Modes

All the GFRP liners failed by ring deflection and wall crushing at springline. Specimens GS-03 and GS-04 delaminated at the crown and underwent wall buckling. The modes of failure for GFRP liners are presented in Figure 3. Initiation of the crack at springline was at 5 kN for all the three specimens. The specimens reached an average peak load of 11.5 kN after which they failed. Since GFRP is a flexible and elastic material, the liners almost returned to its original shape and size after unloading.

Figure 3: Modes of failure for GFRP liner (a) ring deflection; (b) cracking at springline; and (c) delamination at crown and wall buckling; and (d) regained shape after unloading

All the CFRP liners failed by ring deflection and cracking at the springline. Most importantly, there was a reversal of curvature at the crown and the invert lifted and cracked for both the specimens. A continuous crackling sound of individual fibers fracturing was observed until the specimens ultimately failed. This acoustic effect of the buckling fibers could have taken place due to brittle nature of carbon fibers under loading. The CFRP liners ultimately failed by brittle fracture. The cracks at springline started occurring at 7.5 kN and specimens reached a peak load of 13 kN averagely. The reversal of curvature was recorded at an average load of 11 kN. Being a stiff material, CFRP partially retained the reversed curvature at crown and lifted invert even after unloading. Figure 4 shows the modes of failure for CFRP liners and its deformed shape after unloading.

Figure 4: Modes of failure for CFRP liner (a) ring deflection; (b) cracking at springline; and (c) reversal of curvature at the crown and lift at invert; and (d) deformed shape after unloading

3.2 Load – Diametrical deflection Behaviour

The results from transverse compressive loading based on the diametrical deflection for the GFRP and CFRP liners are given in Table 2. Load vs diametrical deflection of the GFRP and CFRP test specimens are shown in Figure 5 (a) and (b), respectively. As mentioned previously, two string potentiometers were used to measure the diametrical deflection in each direction and the average of two was used for further calculations. However, the data from the two devices were very close to each other.

Table 2: Summary of test results based on diametric deflection

Specimen Type	Peak Load (kN)		Vertical Deflection at Peak Load (mm)		Horizontal Deflection at Peak Load (mm)	
	AVG	SD	AVG	SD	AVG	SD
GS	11.50	1.40	186.90	15.70	117.00	5.50
CS	13.00	0.12	63.50	27.80	42.80	13.90

Note: AVG: Average; SD: Standard Deviation

From Figure 5 (a) and (b) it can be observed that the GFRP specimens behave almost linearly until an average load of 8 kN and CFRP specimens until 11kN, and then they behave non-linearly until they reach the peak load. As the load increases, the deflections become large and the specimens start becoming more elliptical, when compared to the original circular cross-section of the liner. This is the source of non-linearity in these specimens and is called geometric non-linearity. As expected, the CFRP specimens had a higher stiffness and peak load when compared to the GFRP specimens and they suffered less deflection.

An analytical model was developed to find the vertical and horizontal deflection as the specimen became more elliptical under loading using an iterative procedure to correspond with test results as presented in the figures below. The model is described in Section 4 of this paper.

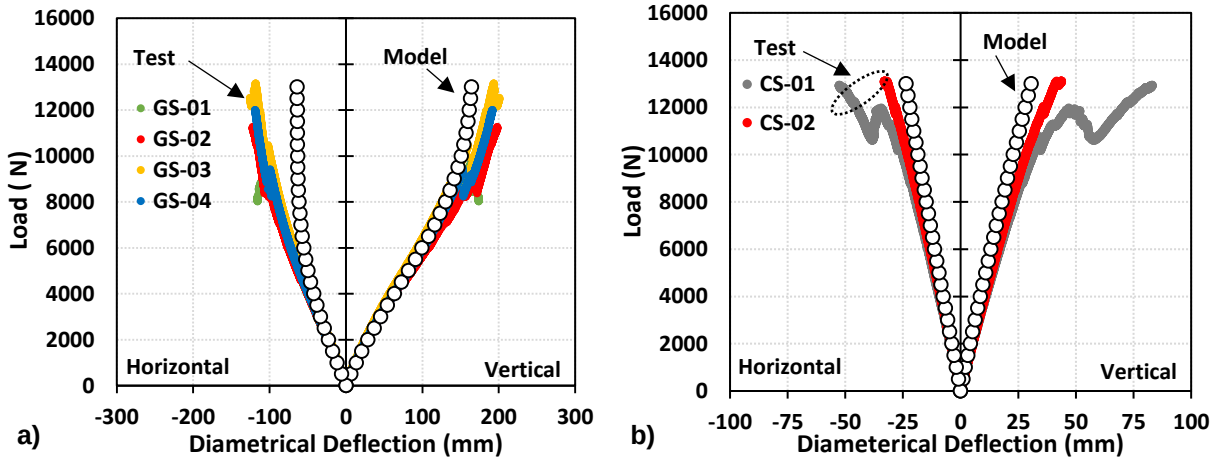

Figure 5: Load vs. diametrical deflection for (a) GFRP and (b) CFRP specimens

3.3 Load – Strain Behaviour

Strain Gauges were used to determine the strain in springline and crown/invert positions. Figure 6 and 7 presents the Load – Strain behaviour of GFRP and CFRP specimens respectively, at the springline and crown/invert positions. Some strain gauges were lost during the test and therefore the curves were continued based on their previous slopes to reach the failure load.

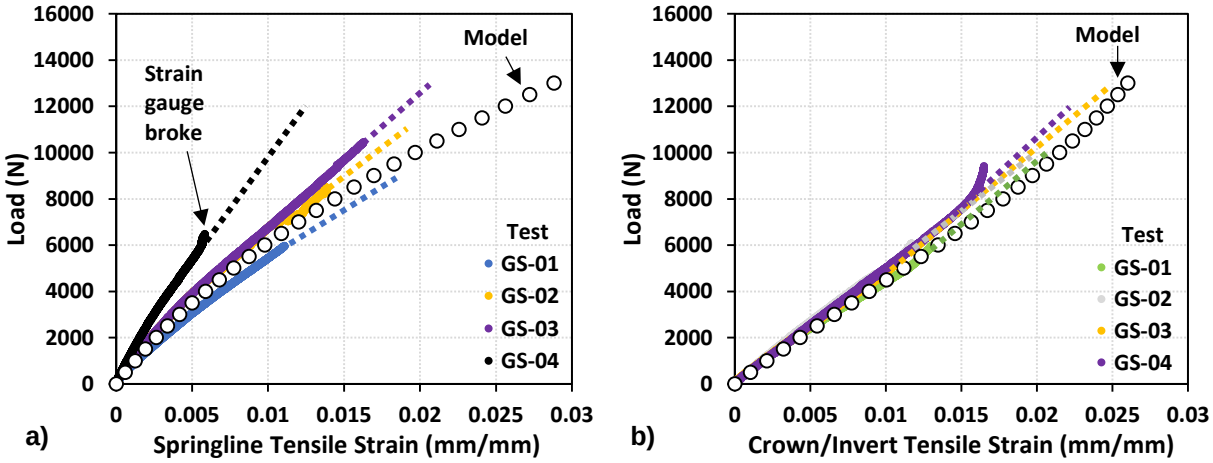

Figure 6: Load vs. strain behavior of GFRP specimens at (a) springline and (b) crown/invert positions

While comparing the load – strain graph of GFRP and CFRP specimens, it is evident that, CFRP has yielded and undergone plastic deformation and that it has a low ductility. Strain in CFRP specimens is significantly lower than the GFRP specimens under their corresponding peak loads. This accounts for the higher stiffness in CFRP liners and high flexibility in GFRP liners. The linear variation in Figure 6 (a) and (b) indicate that the GFRP specimens showed less or no yielding and it is difficult to permanently deform this material under compressive loading. It is also noticeable that the strain for a given load is higher at the crown/invert than the springline. This is because, both GFRP and CFRP specimens undergo maximum deflection in the vertical direction when compared to the horizontal direction.

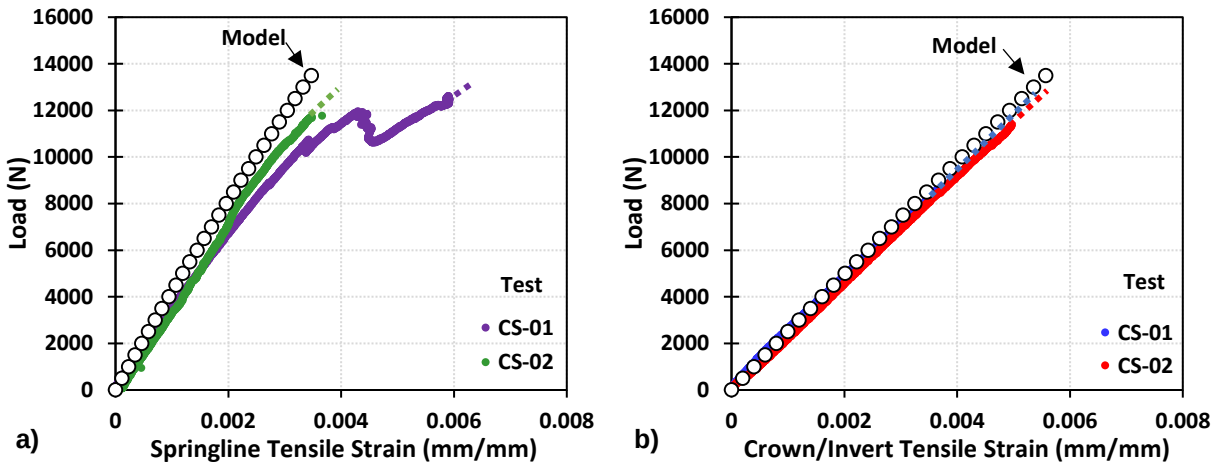

Figure 7: Load vs. strain behavior of CFRP specimens at (a) springline and (b) crown/invert positions

3.4 Pipe Stiffness and Stiffness Factor

Pipe stiffness (PS) is the ratio of force per unit length of the specimen (F) to the deflection in pipe diameter (Δy) as expressed in equation 1. It is the slope of the load-deflection diagram. In general, the pipe stiffness at 5% vertical deflection is used as the stiffness for design purposes.

[1] $PS = {}^{F}/_{\Delta y}$

The stiffness factor (SF) is the product of PS and the quantity 0.149 r^3, which is derived using basic mechanics relating to the total strain energy stored in a ring specimen. The expression for SF is given in equation 2 where, E is the elastic modulus and I is the moment of inertia. In this study, the PS and SF for all the specimens were calculated at 5% and 10% vertical deflection and averaged as shown in Table 3.

[2] $SF = EI = PS \times (0.149\ r^3)$

Table 3: Summary of Test Results based on PS and EI

Specimen Type	PS at 5% vertical deflection (MPa)		PS at 10% vertical deflection (MPa)		EI at 5% vertical deflection (kN-mm²/mm)		EI at 10% vertical deflection (kN-mm²/mm)	
	AVG	SD	AVG	SD	AVG	SD	AVG	SD
GS	0.25	0.01	0.23	0.01	172.94	11.05	159.87	8.92
CS	1.13	0.04	1.03	0.06	847.21	23.21	765.66	41.47

A model EI was developed using cross-sectional analysis of the solid wall section. The EI based on test data was compared to the model EI and the results are as shown in Table 4.

Table 4: Comparison of model EI and EI based on test

Specimen Type	Model EI (kN-mm²/mm)	EI at 5% vertical deflection / EI model	EI at 10% vertical deflection / EI model
GS	173.13	0.999	0.923
CS	918.64	0.922	0.833

It can be observed from Table 4, that EI at 5% vertical deflection shows high compatibility with model EI as expected, for both specimen types. The model EI is based on the results from tensile coupon test. Ply thickness of the coupon was used to find the normalized elastic modulus and the second moment of area was calculated based on the section properties. The model flexural rigidity was calculated per unit width.

4 OVERVIEW OF ANALYTICAL MODEL

4.1 Vertical and Horizontal Deflection

An analytical model was developed to account for the elliptical deformation that the liner specimens undergo due to transverse compressive loading. This model was generated using basic mechanics and further iterated using Mathcad software. The liner was considered as a 2-dimensional ring section, which was subjected to concentrated compressive forces. Due to symmetry, only a quarter of the ring was used to model the deflections. Figure 8 shows the free body diagram of the elliptical ring with bending moments and local constraints used to calculate the vertical deflection. Since the magnitude of bending moment M_A is statically indeterminate, Castigliano's theorem was used to find it. Displacement corresponding to M_A is zero, since there is no rotation at A. This is given in equation 3, where U is the strain energy of the quadrant of the ring.

[3] $\frac{dU}{dM_A} = 0$

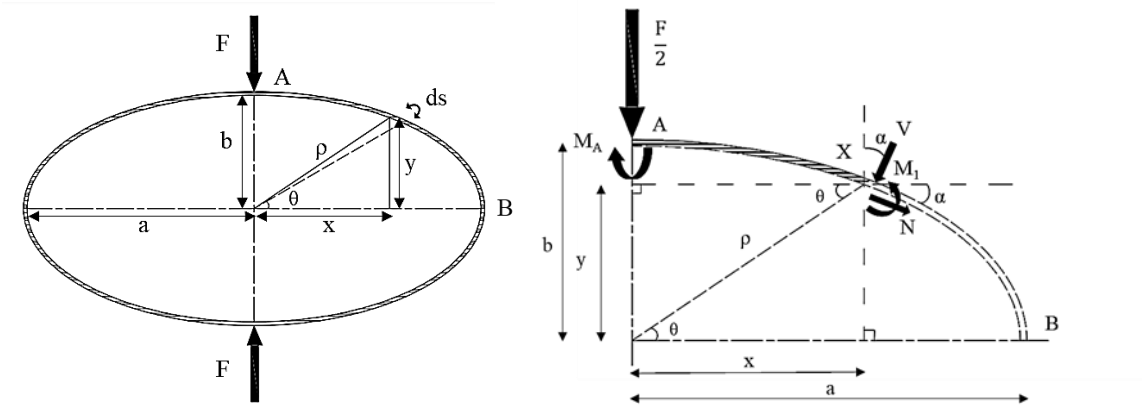

Figure 8: Free body diagram of the elliptical ring to calculate vertical deflection

At point X, the moment equilibrium is as given in equation 4 where, ρ is the radius of the curvature of the ellipse which is presented in equation 5. The strain energy, U in equation 6 is differentiated with respect to F to find the vertical deflection.

[4] $M_1 = M_A - \frac{F}{2} \rho \cos\theta$

[5] $\rho = \frac{a \cdot b}{\sqrt{b^2\cos^2\theta + a^2\sin^2\theta}}$

[6] $U = \frac{2}{EI}\int_0^{\pi/2} {M_1}^2 \rho \, d\theta$

The vertical deflection is given in equation 7, where K_1 is an integral obtained by differentiating U with respect to M_A.

[7] $\delta V = K_1 \left(\frac{F}{EI}\right)$

Similarly, the horizontal deflection was determined by considering two equally opposite imaginary forces, Q in the horizontal direction. The free body diagram of the elliptical ring to calculate horizontal deflection is given in Figure 9. In this case, the moment M_2 and horizontal deflection δH are as given in equation 8 and 9. K_2 in equation 9 is an integral obtained from differentiating U with respect to M_A and M_B. To find the horizontal deflection, overall moment M is considered as the sum of M_1 and M_2, and the strain energy is differentiated with respect to Q.

[8] $M_2 = M_B + \frac{Q}{2} \rho \sin\theta$

[9] $\delta H = K_2 \left(\frac{F}{EI} \right)$

Overall, the model deflection seemed to be in good agreement with the test deflection. For the CFRP liners, the model perfectly co-ordinated with the test deflection until the load, where the liners showed linear variation. For the GFRP specimens, the curves were not as linear and steeper as CFRP, since their flexural stiffness is low. An iterative process where a load of 500 N was added at the end of every iteration in the engineering math software, to obtain the new radius of curvature based on the elliptical ring deflection the specimens undergo due to loading, was adopted to show the geometric non-linearity.

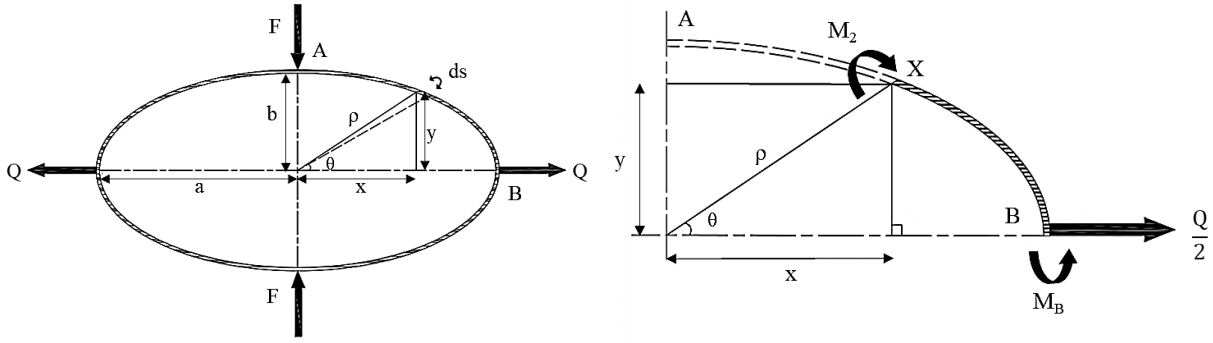

Figure 9: Free body diagram of the elliptical ring to calculate horizontal deflection

4.2 Strain at Springline and Crown/Invert

The tensile strain at springline and crown/invert were determined using basic stress formula as presented in equation 10 and elastic modulus. A free body diagram of the elliptical ring to calculate the tensile strains is given in Figure 8. The longitudinal force N and shearing force V were determined and are presented in equations 11 and 12 respectively. The corresponding strain at springline and crown/invert after each iteration, was used to plot the load-strain graphs. δV and δH were added to the original curvature at every stage and iterated consecutively.

[10] $\sigma = \frac{N}{A} \pm \frac{Mc}{I}$

[11] $N = -\frac{F}{2} \sin\alpha$

[12] $V = N \cot\alpha$

As shown in Figure 6 and 7, the analytical model matches the test results. It is noticed that GFRP shows non-linear load-strain behaviour while for CFRP which shows linear behaviour. This indicates that as GFRP deflects greatly and is tough when compared to CFRP which is stiff and rigid, due to its low elastic modulus. This high level of elasticity allows it to deform to a larger extent, which thereby causes geometric non-linearity and is clearly visible in the graphs. This is a research is in progress and more liners with different geometrical and material properties applied to concrete pipes will be studied for an in-depth understanding of the system.

5 CONCLUSION

In this study, the performance of GFRP and CFRP liners having an average internal diameter of 330 mm and 360 mm respectively and width of 315 mm under transverse compressive loading was assessed. A custom-made parallel plate test machine was set up, to measure the vertical and horizontal diametrical deflection and tensile strain at springline and crown/invert position. A model was developed to account for the elliptical ring failure and their corresponding tensile strains. Both the liners undergo elliptical ring failure while loading. This will prevent the original pipe structure from failing easily. GFRP being highly flexible, keeps deflecting significantly until it fails. CFRP being highly stiff and having a high elastic modulus, can sustain very heavy loads before it undergoes failure. Both these liners can be used in strengthening existing pipes that are in the end of its service life based on project requirements. The analytical model was in good accordance with the test results. It could encompass the concept of elliptical ring failure which was one of the governing failure modes and could account for the geometric non-linearity of the liner under loading due to large deformations. It was developed using basic mechanics and it substantiated for the higher flexural stiffness of CFRP liners and the elasticity of GFRP liners. The model EI developed based on the cross-sectional analytics and the test EI matched with an accuracy of 99.9% and 92.2% for GFRP and CFRP liners respectively. The optimum vertical deflection to find the SF was found to be at 5% diametrical deflection. Both the liners are seamless and have very less thickness but have good stiffness properties and can carry heavy loads. This method of rehabilitation will therefore be effective and not affect the discharge of conveyance materials and simultaneously reduce the cost of maintenance.

ACKNOWLEDGEMENTS

The authors would like to thank the summer undergraduate student, Aidan McCracken who initially fabricated and strain gauged the liners with the help of the graduate students: Daina MacEachern and Dillon Betts at Dalhousie University, Canada. The authors would also like to thank the efforts by Jordan Maerz and Jesse Keane, technicians at Department of Civil and Resource Engineering, Dalhousie University, who helped with the test setup, instrumentation and testing process. In addition, the authors would like to acknowledge QuakeWrap Inc. (Tucson, AZ, USA) for providing the glass and carbon fabric and epoxy resin which was used for the fabrication.

REFERENCES

ASTM D2412. 2011.*Standard Test Method for Determination of External Loading Characteristics of Plastic Pipe by Parallel-Plate Loading*, American Society of Testing and Materials International, West Conshohocken, PA, USA.

Simpson, B, Hoult, N A and Moore, I D. 2017. Rehabilitated reinforced concrete culvert performance under surface loading. *Tunnelling and Underground Space Technology,* **69**:52-63.

Hiroshi, F, Tetsuya, W and Masaaki, I, Atsushi. 2002. Compression bending test for CFRP pipe. *Composites Science and Technology,* ELSEVIER, **62**(15): 2075-2081.

Lee, D C and Karbhari, V M. 2005. Rehabilitation of Large Diameter Prestressed Cylinder Concrete Pipe (PCCP) with FRP Composites — Experimental Investigation. Advances in Structural Engineering, SAGE Journals, **8**(1): 31-44

Park, J, Hong, W, Lee, W, Park, J and Yoon, S. 2014. Pipe Stiffness Prediction of Buried GFRP Flexible Pipe. *Polymers & Polymer Composites*, SAGE Journals **22**(1): 17-23.

Rafiee, R and Habibagahi, M. 2018. Evaluating mechanical performance of GFRP pipes subjected to transverse loading. *Thin-Walled Structures,* ELSEVIER, **131**: 347-359.

Rafiee, R and Habibagahi, M. 2018. On The Stiffness Prediction of GFRP Pipes Subjected to Transverse Loading. *KSCE Journal of Civil Engineering,* **22**(11): 4564-4572.